Nanoscale

PAPER

Cite this: *Nanoscale*, 2015, **7**, 5403

In situ nanomechanical characterization of the early stages of swelling and degradation of a biodegradable polymer†

A. C. Dumitru,[a] F. M. Espinosa,[a] R. Garcia,*[a] G. Foschi,[b] S. Tortorella,[c] F. Valle,[c] M. Dallavalle,[d] F. Zerbetto[d] and F. Biscarini[b,c]

Received 13th January 2015,
Accepted 12th February 2015

DOI: 10.1039/c5nr00265f

www.rsc.org/nanoscale

The interactions of a biodegradable scaffold with cells or living tissues depend on the time-evolution of the nanoscale properties of the scaffold. We present an *in situ* quantitative study on the early-stage swelling and degradation of poly(lactic-*co*-glycolic acid) (PLGA). A novel metrology scheme based on force microscopy measurements of the patterns of PLGA nanostructures is developed to characterize the evolution of topography, volume and nanomechanical properties. The volume and nanoscale roughness show an oscillating behaviour during the first eight days of immersion; at a later stage, we observe a continuous decrease of the volume. The effective Young's modulus exhibits a monotonic decrease from an initial value of about 2.4 GPa down to 9 MPa at day 14. The oscillating behaviour of the volume before the onset of full degradation is explained by a coupled diffusion-swelling mechanism. The appearance of a second maximum in the volume evolution results from the competition between swelling and degradation.

Introduction

Poly(lactic-*co*-glycolic) acid (PLGA) is a biocompatible and biodegradable[1–4] polymer, which has been widely used for biomedical applications such as drug release particles and films, sutures, artificial skin grafts, substrates for cell proliferation and implants.[5–9]

One of the key features of this polymer is the fact that it undergoes hydrolytic degradation[10,11] of the ester backbone in aqueous medium and the resulting products (lactic and glycolic acid) are metabolized and eliminated. The applications of PLGA depend strongly on the dynamics of scaffold degradation. Efforts have been made to understand and control the mechanism of PLGA degradation in relation with the structure and morphology, chemical architecture, the processing method of the material and also the medium in which the polymer is placed.[12–14] However, the dynamics of PLGA degradation and the factors which influence it are not fully understood, consequently, it is hard to predict the degradation process *in vitro* and *in vivo*.

Understanding the correlation between the properties of nanoscale and macroscale materials is a key issue to improve the performance of materials and devices.[15–17] Several techniques that have been employed for studying the changes that biodegradable scaffolds undergo upon degradation cannot be used *in situ* or in a liquid environment.[18–20] Moreover, most of the methods are designed for the evaluation of bulk properties of polymer samples.

Atomic force microscopy and spectroscopy methods provide high resolution approaches to characterize the topography and the mechanical response of soft-matter interfaces in air and buffer.[21–25]

Here, we perform a high resolution nanomechanical characterization of the early stages of swelling and degradation of a PLGA 75 : 25 copolymer in phosphate buffered saline (PBS). To follow the changes of PLGA over 14 days with nanoscale positioning accuracy, we have used micro- and nanoscale PLGA patterns fabricated by focused ion beam lithography. Force microscopy and spectroscopy methods have been used to follow the *in situ* evolution of those patterns. The evolution of the morphological properties, size and surface roughness shows two different periods. The first period, from day 0 to day 8, shows alternating changes in the volume. The second period, from day 9 until day 14 shows a slow reduction of the

[a]*Instituto de Ciencia de Materiales de Madrid, CSIC, c/Sor Juana Inés de la Cruz 3, 28049 Madrid, Spain. E-mail: r.garcia@csic.es*
[b]*Life Sciences Dept., Università di Modena e Reggio Emilia, Via G. Campi 183, 41125 Modena, Italy*
[c]*Consiglio Nazionale delle Ricerche (CNR), Istituto per lo Studio dei Materiali Nanostrutturati (ISMN), Via P. Gobetti 101, 40129 Bologna, Italy*
[d]*Dipartimento di Chimica "G. Ciamician", Università di Bologna, V. F. Selmi 2, 40126 Bologna, Italy*
†Electronic supplementary information (ESI) available. See DOI: 10.1039/c5nr00265f

volume of the PLGA structures. On the other hand, the elastic response of the PLGA shows a continuous softening upon immersion in PBS. The Young's modulus shows a 200-fold decrease from an initial value of 2.4 GPa to 9 MPa. The softening rates have two high regions that match the days when the volume shows higher increase.

Experimental methods

Materials and reagents

Poly(D,L-lactide-*co*-glycolide) 75 : 25 and molecular weight of M_W = 66 000–107 000 g mol^{-1}, phosphate buffered saline powder which yields 0.01 M phosphate buffered saline (NaCl 0.138 M; KCl 0.0027 M) when dissolved in 1 liter of water, chloroform, 2-propanol, ethanol, (3-aminopropyl)triethoxysilane (APTES), ammonium hydroxide solution (28.0–30.0% NH_3), and hydrogen peroxide were all purchased from Sigma Aldrich.

PLGA patterned surfaces

Silicon substrates have been cleaned with 2-propanol, acetone and distilled water by ultrasonic treatment for 5 minutes each. The substrates were then immersed in a H_2O_2–NH_4OH–H_2O (1 : 1 : 2) mixture and four ultrasound cycles of 10 minutes have been performed. After the cleaning procedure, the substrates were immersed in a solution containing 11 μl APTES and 50 mL ethanol for 45 minutes. Finally, the substrates were rinsed with ethanol and water, and dried under N_2. PLGA 75 : 25 was dissolved in chloroform (2% wt) and spin coated at 5400 rpm for 120 s onto the APTES-functionalized silicon substrate. The solvent was allowed to evaporate at room temperature for 24 hours before further processing of the samples.

An IonLiNE (Ion beam Lithography, Nanofabrication and Engineering Workstation RAITH GmbH, Germany) focused ion beam apparatus was used to obtain the patterned surfaces onto silicon. The aperture used was of 70 μm, the intensity of the Ga^+ ions was 132 pA and the dose was 20 000 μC cm^{-2} in 10 loops. The size of the patterned area was 25 μm × 25 μm.

AFM analysis

The experiments were performed using a multimode atomic force microscope fitted with a Nanoscope V Controller (Brucker, Santa Barbara). The images have been obtained in the amplitude modulation AFM mode (repulsive regime).[26] The free amplitude A_0 was 20 nm and the set-point amplitude A_{sp} was 10 nm. At day 0, the PLGA samples were characterized (topography and mechanical response) in air and then immersed in PBS buffer. During the 14 days, the samples were analysed in PBS on a daily basis in order to follow the changes in morphology and mechanical properties.

Topography analysis of the PLGA patterns. Images and force curves were recorded in both air and PBS environment. Rectangular PPP-NCH (Nanosensors, Switzerland) cantilevers with a nominal force constant k = 40 N m^{-1} and a resonance frequency of 291 kHz have been used for air measurements.

For the experiments performed in PBS buffer, rectangular PPP-FM (Nanosensors, Switzerland) cantilevers with a nominal force constant k = 2.8 N m^{-1} and resonance frequency of 75 kHz were employed. The microscope is equipped with a liquid cell where approximately 60 μl of PBS at pH 7.4 are introduced in order to carry out the measurements. The topography measurements were performed using amplitude modulation AFM by driving mechanically the cantilever.[27]

Nanomechanical spectroscopy. Nanomechanical spectroscopy refers to the determination of the mechanical properties such as the Young's modulus with nanoscale spatial resolution from AFM observables.[24,28–30] The nanomechanical measurements involve the accurate determination of the cantilever force constant as well as the optical lever sensitivity. The force constant and quality factor are determined by using the thermal noise method.[31] In order to calibrate the optical lever sensitivity, we acquired deflection *versus* distance curves on a hard surface (muscovite mica). Typically, 100 deflection *versus* distance curves were acquired and the sensitivity of the photodiode was calculated from the mean value of the slope of the above mentioned curve in the repulsive region.

The force curves were obtained in contact mode by approaching and retracting the tip towards the sample 300 nm at 1 Hz. Each curve has 1024 points. Once the deflection *versus* piezo-displacement curves are obtained, the curves are converted into force *versus* indentation curves by applying Hooke's law; $F = -kd$ (d is the cantilever deflection, k is the cantilever force constant). Finally, the indentation δ is calculated by taking the difference between the piezo-displacement and the tip deflection.[29] Typical indentation levels were maintained below 10 nm (which corresponds to roughly 10% of the thickness of the PLGA film) to minimize the contribution of the substrate to the mechanical response of the material.

The Young's modulus was derived using the Sneddon model for a paraboloid probe,[32] where F is the applied load, R is the curvature radius of the probe apex, E is the effective Young's modulus of the material, ν is the Poisson ratio (0.3 for polymeric materials):

$$F = \frac{4}{3}\frac{E}{(1-\nu^2)}R^{1/2}\delta^{3/2} \quad (1)$$

The Young's modulus is computed from the slope of eqn (1).

Swelling model

In order to model the experimental data closely, we applied a numerical approach. The backbone of the model is based on Peppas *et al.*'s studies.[33] The model explicitly describes swelling. It is able to portray a range of diffusional behaviour, from Fickian to Case II.[34,35] Non-ideal concentration effects on the diffusion coefficient can be included. The model is solved numerically using the finite element methodology[36]

The basis of the model is Fick's law;

$$\frac{\delta C}{\delta \tau} = \frac{\delta}{\delta \xi}\left(D\frac{\delta C}{\delta \xi}\right) \quad (2)$$

where C is the normalized concentration of the solvent;

$$C = \frac{C_w}{C_{w,e}} \quad (3)$$

with C_w as the local (non-equilibrium) concentration and $C_{w,e}$ as the equilibrium concentration of the solvent. The spatial coordinate, x is normalized with respect to the dry polymer thickness, L_0 (4) and the penetrant diffusion coefficient D normalizes the time scale (5);

$$\xi = \frac{x}{L_0} \quad (4)$$

$$\tau = \frac{Dt}{{L_0}^2} \quad (5)$$

The coefficient D is described by the Fujita-type exponential $D(C) = \exp[-\beta(1 - C)]$, where β is a parameter that defines the concentration dependence of D. The layers are allowed to expand as a function of the amount of the solvent. The material swelling is described by the three equations. Initially the swelling follows:

$$\Delta\xi_i = \frac{\Delta\xi_0}{1 - \nu_e \cdot C_i} \quad (6)$$

with i = 1, 2,..., 20, being the index of the 20 spatial domains in which the polymer is sub-divided for computational purposes; ν_e is a material constant. Eqn (6) describes swelling at early times, specifically for the first time region. In the second time region the polymer relaxes as:

$$\Delta\xi_i = \alpha\tau^b \quad (7)$$

with α = 1.12 and b = 0.21, while for longer times, we consider

$$\Delta\xi_i = \left(\frac{{\Delta\xi_0}^3}{1 - \nu_e \cdot C_i}\right)^{1/3} \quad (8)$$

with the material constant ν_e = 0.76.

Full details of the numerical solution are found in the ESI.†

Results

To follow, measure and understand the changes experienced by the PLGA upon immersion in PBS, we performed two types of measurements. First, we used the AFM to map the topographical changes at the nanoscale as a function of the immersion time in the buffer environment. Second, we measured the changes of the elastic response (Young's modulus) of the scaffold. The measurements are performed over 14 days. That period has been chosen in view of potential applications of PLGA as the scaffold to attach cells. Many cells have maturation and proliferation periods of 7 to 14 days.[37]

Topography and nanomechanical properties of PLGA samples before incubation in PBS

The samples have been analyzed in air at room temperature prior to the immersion in PBS buffer. An array of PLGA rectangular structures separated by 2.5 μm was fabricated on silicon by using focused ion beam lithography (Fig. 1A). Each PLGA pattern has an area of 1.5 μm × 1 μm and a height of 100 nm (Fig. 1B). A cross-section of a single PLGA pattern is shown in Fig. 1C. The peak at the edges of the pattern is a result of the lithography process.

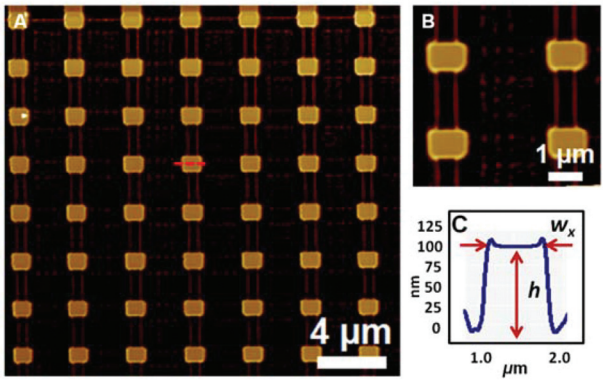

Fig. 1 AFM topography images of a PLGA nanopattern on a silicon substrate. (A) 25 μm × 25 μm area of PLGA patterns on silicon. (B) Zoomed image of four PLGA patterns. (C) Cross-section of a PLGA pattern.

This kind of pattern facilitates the measurement of the surface topography, the volume changes and the mechanical response of the same region with a spatial accuracy in the sub-100 nm range. The measurements included here represent an average of 8 different PLGA patterns.

Topography evolution of PLGA structures in PBS

Patterned PLGA samples have been immersed in PBS buffer of pH 7.4 at room temperature. The samples have been analyzed on a daily basis for 14 days in the same liquid environment. At the end of each day, the buffer solution was refreshed. The evolution of the width and height of the same PLGA structure is presented in Fig. 2. The time evolution graphs show two distinctive regions. First, the height and width show an oscillating behavior that ends at day 8. Then, both height and width decrease with the immersion time. The pattern doubles its width after the first day of immersion. In addition, during the whole period studied here, the width of the PLGA structure was wider than the original value. The changes in height are in the 5–15% range with respect to the dry pattern. The alternating increase/decrease behavior has also been observed in macroscopic PLGA samples.[20,38] The data show higher variations in width as compared to height.

Fig. 3 shows the evolution of the volume ($w_x \times w_y \times h$) with the immersion time. The volume reproduces the same behaviour shown above, that is, the volume shows a sharp increase during the first 24 hours of immersion, which is followed by a relatively slow decrease (day 2 to day 4), then it increases over the following 4 days and thereafter, the volume decreases.

To better visualize the volume evolution, the volume has been normalized to its initial (dry) volume. At the end of the 14 days in PBS, the pattern shape was conserved although the

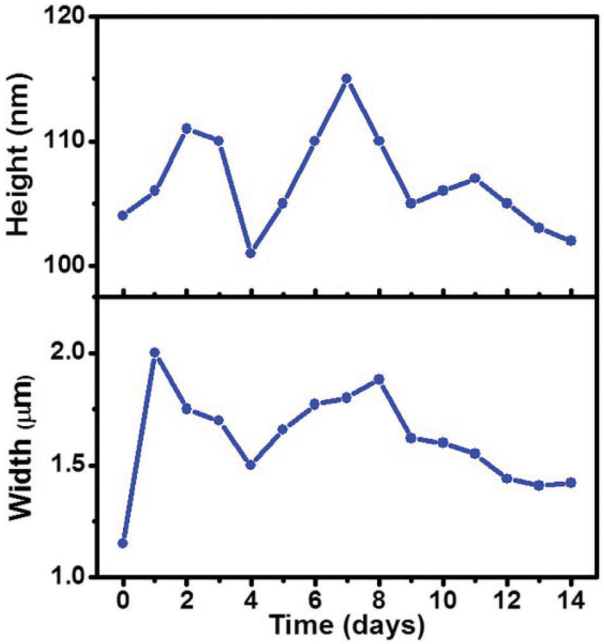

Fig. 2 Evolution of the height and width of a single PLGA pattern as a function of the days immersed in PBS. The values represent an average of 8 different patterns.

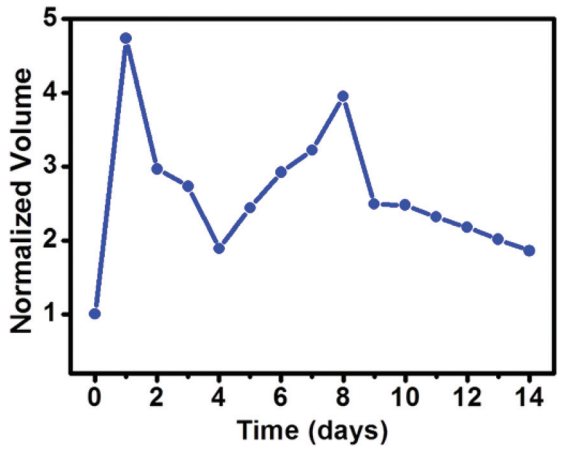

Fig. 3 Evolution of the volume of the PLGA patterns upon immersion in PBS. The values are normalized with respect to the initial value of the dry volume in air (V_{air} is 0.097 μm^3) and they represent an average of 8 different patterns.

volume showed a 2-fold increase. The volume changes of the PLGA structure at its peak value represent a 4-fold increase.

We have also measured the surface roughness over the top section of the PLGA structures (approximately 1 μm^2) (Fig. 4). The overall behaviour reproduces the oscillating behaviour noted above. A sharp increase after the 1st immersion day is followed by a quick decrease during the 2nd day. This is followed by an overall increase that peaks between days 6 and 8. After that, the roughness decreases for two additional days and then there is a small increase. We note that immersion in PBS, independent of the number of immersion days, increases

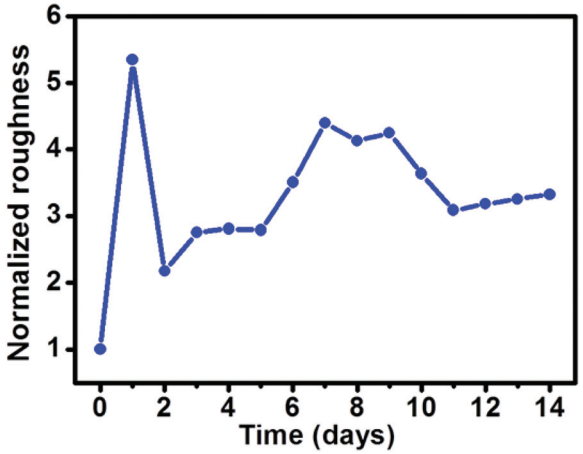

Fig. 4 Normalized roughness of the surface of PLGA patterns as a function of immersion time in PBS. Roughness values (rms) have been normalized with respect to the rms value obtained in air before immersion in PBS (rms_{air} = 0.52 nm).

the roughness with respect to the dry sample. After the first day, the roughness (rms value) has a 5-fold increase. At the end of the period studied here, the rms shows a 3-fold increase with respect to the dry PLGA surface.

We have also studied the evolution of the surface topography of the PLGA pattern by performing amplitude modulation AFM measurements in the repulsive regime. Fig. 5 depicts the surface topography of the same pattern before and during immersion in PBS. Prior to PBS immersion, the pattern shows considerable height changes (Fig. 5A). Those height variations across the pattern surface are significantly reduced after immersion in PBS (Fig. 5B and C).

Nanomechanical analysis of the PLGA patterns

The nanomechanical analysis of the PLGA structures has been carried out both before immersion in PBS and also every day during 14 days (Fig. 6). The values of the Young's modulus are normalized with the value obtained in air at day 0. Initially, (air) the Young's modulus is about 2.4 GPa. An important drop of the Young's modulus down to around 200 MPa is observed when the sample is immersed in PBS. The steady decrease continues until around day 7, when it reaches 17 MPa. From this point onwards, the Young's modulus decreases and small fluctuations are observed between days 11 and 14.

The decrease of the Young's modulus is marked by the presence of two regions with higher slopes, one during the 1st day of immersion and the other between days 6 and 7. Those days coincide with the times when the morphological features of the patterns show a fast increase.

Discussion

The experimental data show oscillations in the volume and roughness which are not present on the changes of the Young's modulus (Fig. 7). The Young's modulus decreases

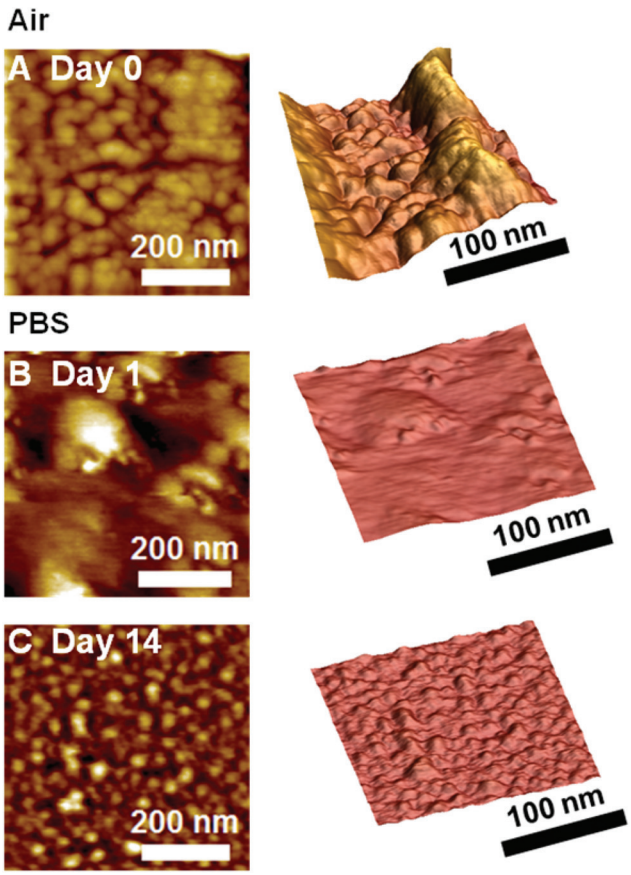

Fig. 5 High resolution topography images of a PLGA nanopattern's top surface. 3-D images are shown for a better visualization of the erosion process. (A) Pattern topography as imaged in air medium before starting the degradation experiment; (B) Image of the PLGA pattern surface taken in PBS buffer after 1 day of incubation; (C) Surface topography of a PLGA pattern measured in PBS buffer on day 14 of immersion.

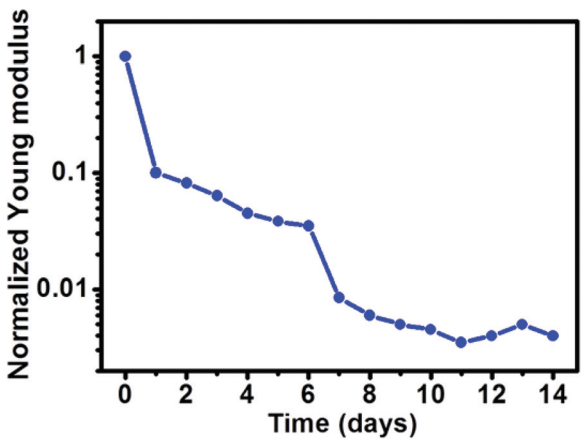

Fig. 6 Evolution of the Young's modulus of the PLGA patterns as a function of the immersion time in PBS. The values are normalized with respect to the initial value of the Young's modulus in the dry state (E_0 = 2.4 GPa) and represent an average of 8 different patterns.

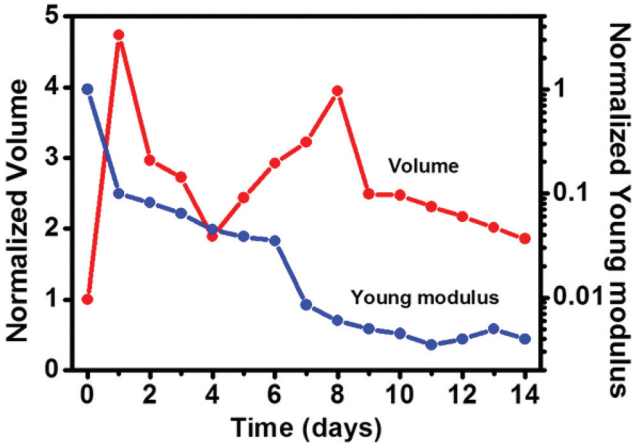

Fig. 7 Young's modulus and volume evolution upon immersion in PBS.

from the first day of immersion. However, the highest decrease of the Young's modulus coincides or is very close to the days when the volume reaches the local maxima.

We have developed a theoretical model to explain the volume changes observed on the PLGA patterns during the first week. Fig. 9 shows the comparison between theory and experimental data. The model describes the width expansion as a function of time by introducing three regimes. Initially, the solvent diffuses into the polymer from the external interfaces. The diffusion coefficient depends on the solvent concentration. The solvent uptake is slow in the unsolvated polymer domain, and it becomes faster in the regions where the polymer has already been solvated. The solvation favours chain rearrangement which leads to a quick increase in the volume (1D diffusion). The presence of solvent molecules triggers internal stress in the polymer which leads to the uncoiling and rearrangement of large segments of polymer chains. This regime involves a volume shrinking (relaxation). Once the stress is removed by viscous flow, further solvent uptake is possible which leads to a second swelling (3D diffusion).

This swelling-deswelling process is accompanied by a decrease of the Young's modulus. The sharp decrease of E in the first 24 hours is correlated with the initial swelling process due the uptake of solvent molecules. The moderate decrease of E observed between day 1 and day 6 is also consistent with the model involving uncoiling of the polymer chains and subsequent filling of the polymer voids. The release of the polymer stress favours the uptake of solvent molecules which causes swelling, which in turn causes a relatively sharp decrease of the Young's modulus.

Certainly, PLGA degradation both due to erosion (Fig. 5) and bulk degradation happens since day 1. However, those processes, in particular, bulk degradation does not seem to dominate the evolution in this period (from day 0 to 7). The degradation of PLGA is caused by hydrolysis of the ester bonds inside the polymeric matrix in the presence of water molecules, with the formation of acidic oligomers and finally monomers (Fig. 8). However, the hydrolysis of the ester links is

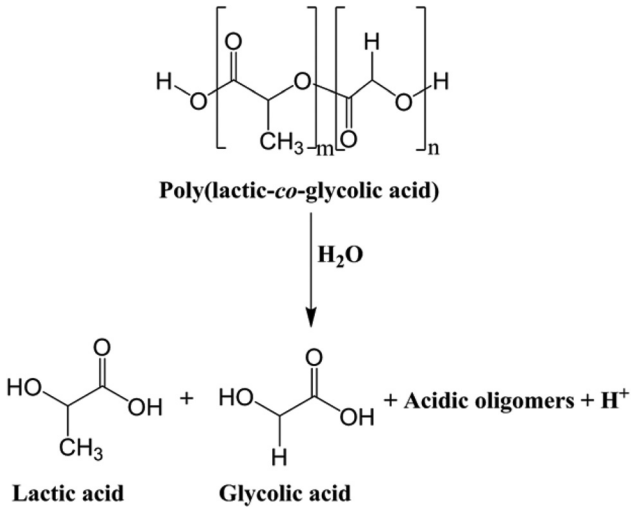

Fig. 8 Chemical structure of poly(lactic-*co*-glycolic acid) and the products of its hydrolytic degradation. In a PLGA copolymer, *m* and *n* refer to the amounts of lactide and glycolide monomer units.

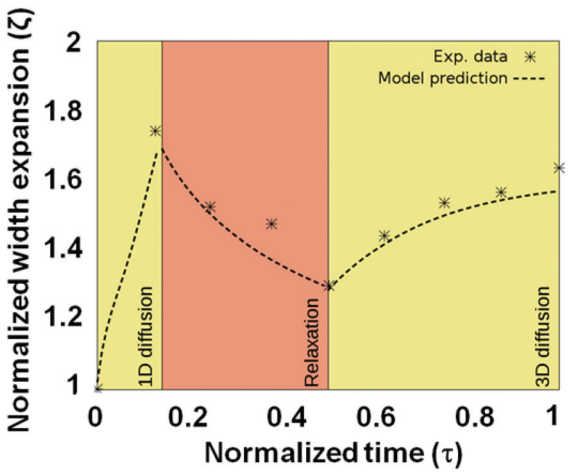

Fig. 9 Normalized width expansion of the PLGA as a function of time. Three regimes of the polymer volume changes are highlighted: (1) initial swelling, (2) relaxation, (3) final swelling. Experimental results are in agreement with the solution of the model, which is plotted as a dashed line.

slower than water diffusion through the material.[14] The initial increase of the volume is induced by water molecules penetrating the polymeric matrix.

The small variation in the volume of the PLGA patterns along with the decreasing tendency of the height observed from day 8 onwards can be interpreted as a result of pore formation inside the polymer matrix and a slow release of oligomers resulted from the hydrolysis of ester bonds. This leads to a small-scale mass loss, which is reflected by a 5% drop in height at day 14 in PBS as compared to the one at day 1. The reported mass loss for 75 : 25 PLGA copolymers in the first two weeks of degradation is between 10 and 20%.[18,39] Interestingly, as mentioned in a recent study on hydrogel particles swelling,[38] the process takes place anisotropically and inhomogeneously. We observe that the PLGA structures swell more in length and width than in height (Fig. 2). This is due to the fact that they are bound to the stiff silicon substrate, which is acting as a constraint on the vertical axis.

In situ measurements of the surface topography at the nanoscale during degradation provide information about the erosion process that takes place at the interface between the PLGA scaffold and the liquid environment. The initial surface displaying significant variations in height is transformed into an eroded area with numerous protrusions and gaps (Fig. 5). Our findings regarding the surface roughness are similar to the ones of Semler *et al.*[40] They have also observed a decrease of the number of regions containing rapid and drastic variations as a result of degradation.

The initial measurements in air show that the material has a relatively high Young's modulus of about 2.4 GPa. This value is in agreement with bulk measurements reported elsewhere.[41] Once the sample is immersed in PBS, a sharp decrease of the mechanical properties is observed along with the swelling of the material. By looking at Fig. 7, we observe that there is a competition between swelling and degradation. From day 1 to 8, significant fluctuations of the volume lead to the conclusion that swelling is the major factor causing the decrease of the Young's modulus. In addition, the reported decrease of the molecular weight of PLGA copolymers upon immersion in PBS[18,20] generates lower molecular weight compounds which are more flexible due to the weakening of the intermolecular bonds inside the polymer chain. As a result, the polymeric matrix is not as tightly packed as in the initial dry state, therefore, this is also a factor which leads to the softening of the material. A comparison of the mechanical response *versus* the molecular weight of poly-lactic and poly-glycolic based polymers also shows that there is a strong dependence on the mechanical properties and the molecular weight.[42] Small fluctuations in the Young's modulus take place between days 9–14, but the tendency to decrease is maintained.

Conclusions

We have reported a high spatial resolution and nanomechanical spectroscopy mapping of the early-stages of the evolution of PLGA structures upon immersion in a biological buffer. The evolution of the morphological properties, size and surface roughness and mechanical properties (Young's modulus) shows four stages. The first stage is characterized by a fast swelling. It also involves a sharp decrease of the Young's modulus. The sudden increase in the volume and roughness observed in the first 24 hours and the observed decrease in the Young's modulus are due to a diffusion process where the diffusion coefficient D depends on the solvent concentration C. The solvent uptake is favoured in the already solvated polymer chains leading to a fast increase of the free volume.

The second stage involves a relaxation process that implies a rearrangement of the polymers chains. The PLGA patterns

decrease in size to reach a local minimum in the volume. The relatively slow volume decrease in this regime is associated with the polymer response to the stress caused by the presence of the solution. The Young's modulus keeps decreasing but at a slower rate.

After the stress is dissipated by the viscous flow of the polymer, the polymer is ready to accept more solvent and a second swelling occurs (third stage). Here the Young's modulus also shows a sharper decrease rate. After this stage, the volume shows a steady decrease which is interpreted as the start of the full degradation of the PLGA. The Young's modulus shows a tendency to decrease, but it is less evident than in the previous stages. At the end of the observation process, the Young's modulus decreases by almost three-orders of magnitude from an initial value of 2.4 GPa to 9 MPa.

The observed results are a consequence of three different processes: coupled diffusion-swelling, degradation and erosion. The coupled diffusion-swelling process lasts for about 1 week. The presence of a second peak in the volume and roughness indicates a competition between swelling and hydrolytic degradation of the ester bonds, and the latter is a thermally activated process that happens at a slower rate than water adsorption.

The significant fluctuations of the surface roughness together with the decrease of the Young's modulus could have implications on cells' adherence and proliferation.

Acknowledgements

This work was founded by the European Union Seventh Framework Programme [FP7/2007–2013] under the grant agreement no. 280772, project iONE-FP7 and MINECO (Spain), project CSD2010-00024.

References

1 J. M. Anderson and M. S. Shive, *Adv. Drug Delivery Rev.*, 1997, **28**, 5–24.
2 K. Yamaguchi and J. M. Anderson, *J. Controlled Release*, 1993, **24**, 81–93.
3 S. E. Gautier, M. Oudega, M. Fragoso, P. Chapon, G. W. Plant, M. B. Bunge and J.-M. Parel, *J. Biomed. Mater. Res.*, 1998, **42**, 642–654.
4 A. A. Ignatius and L. E. Claes, *Biomaterials*, 1996, **17**, 831–839.
5 C. J. Ke, T. Y. Su, H. L. Chen, H. L. Liu, W. L. Chiang, P. C. Chu, Y. N. Xia and H. W. Sung, *Angew. Chem., Int. Ed.*, 2011, **50**, 8086–8089.
6 M. L. Chen, S. Gao, M. D. Dong, J. Song, C. X. Yang, K. A. Howard, J. Kjems and F. Besenbacher, *ACS Nano*, 2012, **6**, 4835–4844.
7 A. Mathew, T. Fukuda, Y. Nagaoka, T. Hasumura, H. Morimoto, Y. Yoshida, T. Maekawa, K. Venugopal and D. S. Kumar, *PLoS One*, 2012, **7**, 10.
8 N. Hild, O. D. Schneider, D. Mohn, N. A. Luechinger, F. M. Koehler, S. Hofmann, J. R. Vetsch, B. W. Thimm, R. Muller and W. J. Stark, *Nanoscale*, 2011, **3**, 401–409.
9 G.-J. Wang, Y.-C. Lin and S.-H. Hsu, *Biomed. Microdevices*, 2010, **12**, 841–848.
10 X. S. Wu and N. Wang, *J. Biomater. Sci., Polym. Ed.*, 2001, **12**, 21–34.
11 I. Grizzi, H. Garreau, S. Li and M. Vert, *Biomaterials*, 1995, **16**, 305–311.
12 E. Vey, C. Roger, L. Meehan, J. Booth, M. Claybourn, A. F. Miller and A. Saiani, *Polym. Degrad. Stab.*, 2008, **93**, 1869–1876.
13 T. G. Park, *Biomaterials*, 1995, **16**, 1123–1130.
14 A. Göpferich, *Biomaterials*, 1996, **17**, 103–114.
15 H. Assender, V. Bliznyuk and K. Porfyrakis, *Science*, 2002, **297**, 973–976.
16 J. G. Goetz, S. Minguet, I. Navarro-LÈrida, J. J. Lazcano, R. Samaniego, E. Calvo, M. Tello, T. Osteso-Ib·Òez, T. Pellinen, A. Echarri, A. Cerezo, A. J. P. Klein-Szanto, R. Garcia, P. J. Keely, P. S·nchez-Mateos, E. Cukierman and M. A. Del Pozo, *Cell*, 2011, **146**, 148–163.
17 M. Chyasnavichyus, S. L. Young and V. V. Tsukruk, *Langmuir*, 2014, **30**, 10566–10582.
18 E. Vey, C. Rodger, L. Meehan, J. Booth, M. Claybourn, A. F. Miller and A. Saiani, *Polym. Degrad. Stab.*, 2012, **97**, 358–365.
19 E. Pamula and E. Menaszek, *J. Mater. Sci. Mater. Med.*, 2008, **19**, 2063–2070.
20 J. K. Perron, H. E. Naguib, J. Daka, A. Chawla and R. Wilkins, *J. Biomed. Mater. Res., Part B*, 2009, **91B**, 876–886.
21 Y. F. Dufrene, D. Martinez-Martin, I. Medalsy, D. Alsteens and D. J. Muller, *Nat. Methods*, 2013, **10**, 847–854.
22 A. Ikai, in *Nano/Micro Biotechnology*, ed. I. Endo and T. Nagamune, Springer, Berlin, Heidelberg, 2010, vol. 119, pp. 47–61.
23 E. T. Herruzo, A. P. Perrino and R. Garcia, *Nat. Commun.*, 2014, **5**, 3126–3204.
24 D. Martinez-Martin, E. T. Herruzo, C. Dietz, J. Gomez-Herrero and R. Garcia, *Phys. Rev. Lett.*, 2011, **106**, 198101.
25 M. Chen, S. R. Nielsen, T. Uyar, S. Zhang, A. Zafar, M. D. Dong and F. Besenbacher, *J. Mater. Chem. C*, 2013, **1**, 850–855.
26 R. Garcia and A. San Paulo, *Phys. Rev. B: Condens. Matter*, 1999, **60**, 4961–4967.
27 E. T. Herruzo and R. Garcia, *Appl. Phys. Lett.*, 2007, **91**, 143113.
28 M. D. Dong, S. Husale and O. Sahin, *Nat. Nanotechnol.*, 2009, **4**, 514–517.
29 H.-J. Butt, B. Cappella and M. Kappl, *Surf. Sci. Rep.*, 2005, **59**, 1–152.
30 S. Zhang, H. Aslan, F. Besenbacher and M. D. Dong, *Chem. Soc. Rev.*, 2014, **43**, 7412–7429.
31 H. J. Butt and M. Jaschke, *Nanotechnology*, 1995, **6**, 1.
32 I. N. Sneddon, *Int. J. Eng. Sci.*, 1965, **3**, 47–57.

33 R. W. Korsmeyer and N. A. Peppas, *J. Controlled Release*, 1984, **1**, 89–98.
34 T. Alfrey, E. F. Gurnee and W. G. Lloyd, *J. Polym. Sci., Part C: Polym. Symp.*, 1966, **12**, 249–261.
35 J. S. Vrentas, C. M. Jarzebski and J. L. Duda, *AIChE J.*, 1975, **21**, 894–901.
36 http://www.comsol.com.
37 C. Gualandi, M. Govoni, L. Foroni, S. Valente, M. Bianchi, E. Giordano, G. Pasquinelli, F. Biscarini and M. L. Focarete, *Eur. Polym. J.*, 2012, **48**, 2008–2018.
38 M. Caldorera-Moore, M. K. Kang, Z. Moore, V. Singh, S. V. Sreenivasan, L. Shi, R. Huang and K. Roy, *Soft Matter*, 2011, **7**, 2879–2887.
39 N. Samadi, A. Abbadessa, A. Di Stefano, C. F. van Nostrum, T. Vermonden, S. Rahimian, E. A. Teunissen, M. J. van Steenbergen, M. Amidi and W. E. Hennink, *J. Controlled Release*, 2013, **172**, 436–443.
40 E. J. Semler, J. S. Tjia and P. V. Moghe, *Biotechnol. Prog.*, 1997, **13**, 630–634.
41 E. Pamula, J. Kokoszka, K. Cholewa-Kowalska, M. Laczka, L. Kantor, L. Niedzwiedzki, G. Reilly, J. Filipowska, W. Madej, M. Kolodziejczyk, G. Tylko and A. Osyczka, *Ann. Biomed. Eng.*, 2011, **39**, 2114–2129.
42 E. Vidović, D. Klee and H. Höcker, *J. Appl. Polym. Sci.*, 2013, **130**, 3682–3688.